# RSC Advances



This is an *Accepted Manuscript*, which has been through the Royal Society of Chemistry peer review process and has been accepted for publication.

Accepted Manuscripts are published online shortly after acceptance, before technical editing, formatting and proof reading. Using this free service, authors can make their results available to the community, in citable form, before we publish the edited article. This Accepted Manuscript will be replaced by the edited, formatted and paginated article as soon as this is available.

You can find more information about *Accepted Manuscripts* in the **Information for Authors**.

Please note that technical editing may introduce minor changes to the text and/or graphics, which may alter content. The journal's standard <u>Terms & Conditions</u> and the <u>Ethical guidelines</u> still apply. In no event shall the Royal Society of Chemistry be held responsible for any errors or omissions in this *Accepted Manuscript* or any consequences arising from the use of any information it contains.



Facile Fabrication of nanostructure NiCo<sub>2</sub>O<sub>4</sub> Supported on Ni Foam for High Performance Electrochemical Energy Storage

Changhui Wang, ab Xiong Zhang, Chen Li, ab Xianzhong Sun, Yanwei Ma\*a

a Institute of Electrical Engineering, Chinese Academy of Sciences, Beijing 100190,

China

b University of Chinese Academy Sciences, Beijing 100049, China

E-mail: <a href="mailto:ywma@mail.iee.ac.cn">ywma@mail.iee.ac.cn</a>

Abstract: An intense research in area of electrochemical energy storage (EES) in the past decade has been inspired by the demand for EES in handheld electric devices, transportation, and storage of renewable energy for the power grid. It becomes necessary to find novel electrode materials with high performance, low cost and advanced electrode architecture to meet the large-scale commercial application in the EES. We developed a facile, green and energy-saving technique to fabricate cost-effective nanostructure NiCo<sub>2</sub>O<sub>4</sub> supported on Ni foam (NiCo<sub>2</sub>O<sub>4</sub>/Ni foam) with unique microstructure. As a binder-free electrode material, a high specific capacitance of 760 F g<sup>-1</sup> was achieved with excellent cyclability at a current density of 1 A g<sup>-1</sup>. In conjunction with the superior electrode architecture, the nanoplate-like NiCo<sub>2</sub>O<sub>4</sub>/Ni foam with optimal performances is prospective to meet to the need of wide commercial application in high-efficient EES. The preparation method may be extended to other metal oxide/hydroxide-based materials with outstanding nanostructure for electronic, magnetic, optical, photochemical, and catalytic applications.

Keywords: nanostructure,  $NiCo_2O_4$ , electrochemical energy storage, electrode material, fabrication.

# 1. Introduction

An intense research in area of electrochemical energy storage (EES) in the past decade has been inspired by the demand for EES in handheld electric devices, transportation, and storage of renewable energy for the power grid. However, the process of commercial application for EES is still prohibitive due to the low performance, high cost or various difficulties in large scale-up fabrication of the electrode materials. Therefore, it becomes necessary to find novel electrode materials with high performance, low cost and advanced electrode architecture. <sup>3,4</sup>

NiCo<sub>2</sub>O<sub>4</sub> has been suggested as a promising cost-effective and scalable alternative since it offers many advantages such as low cost, high theoretical capacitance. The preparation techniques include coprecipitation,<sup>5</sup> combustion,<sup>6</sup> hydrothermal method,<sup>7</sup> thermal decomposition,<sup>8</sup> sol-gel process,<sup>9</sup> etc.. Moreover, in general, the active material need to be mixed with a conductive agent and a binder to make a paste and applied to current collectors for electrochemical evaluation.<sup>10,11</sup> Apparently, the complex fabrication process makes it much more difficult to boost the performance and scale-up of the active electrode materials. An emerging advanced technique is to grow electroactive nanostructure materials on conductive substrates to be directly used as binder-free electrodes for EES, such as single-crystalline NiCo<sub>2</sub>O<sub>4</sub> nanoneedle arrays, NiCo<sub>2</sub>O<sub>4</sub> nanowire arrays, or ultrathin mesoporous NiCo<sub>2</sub>O<sub>4</sub> nanosheets supported on Ni foam or Ti foil, <sup>12-14</sup> by one-step hydrothermal method, <sup>12</sup> or multi-step synthetic process including

potentiostatical deposition, <sup>13</sup> or chemical bath deposition (CBD)<sup>14</sup> followed by thermal transformation. <sup>13,14</sup> The electrode design avoids tedious procedure of mixing and coating of the slurry, and makes the active electrode materials free of auxiliary components like conductive agents and binders besides plenty of "dead surface". While the NiCo<sub>2</sub>O<sub>4</sub>-based electrode materials obtained via the above routes have displayed high performance, there still exists a long run in the commercial application for NiCo<sub>2</sub>O<sub>4</sub> in EES, because their synthetic methodologies suffer high energy costs, an elevated temperature, complex equipments, complicated techniques, environmental pollution or low yield, etc..

In this work, we report a facile, green approach to grow nanostructure  $NiCo_2O_4$  on Ni foam ( $NiCo_2O_4/Ni$  foam) with optimal microstructure as a binder-free electrode material for EES. The as-fabricated nanoplatelet-like  $NiCo_2O_4/Ni$  foam possessed a high specific capacitance of 760 F g<sup>-1</sup> at a current density of 1 A g<sup>-1</sup> and an excellent cyclability, remaining over 96.3 % after 1000 cycles, at a high load mass of 1.46 mg cm<sup>-2</sup>. Benefitting from the superior electrode architecture, the high performance nanostructure  $NiCo_2O_4/Ni$  foam is prospective to meet to the need of wide commercial application in high-efficient EES.

## 2. Experimental

#### 2.1. Materials

Ni(NO<sub>3</sub>)<sub>2</sub> 6H<sub>2</sub>O ( $\geq$ 98.0), Co(NO<sub>3</sub>)<sub>2</sub> 6H<sub>2</sub>O ( $\geq$ 99.0), NaOH ( $\geq$ 96.0%) and ethylene glycol (EG,  $\geq$ 96.0%) were used as source materials without further purification. Nickel foams (purity:>99.5%) were cleaned ultrasonically in a 37 wt % HCl solution for 5 min and washed with deionized water and ethanol, before being dried in an oven at 60 °C. <sup>15</sup> All of the regents were analytical grade.

# 2.2. Preparation of the nanostructure NiCo<sub>2</sub>O<sub>4</sub>/Ni foam

In our synthesis process, two steps are involved: (1) preparation of the precursor ethylene glycol intercalated cobalt and nickel layered double hydroxide nanosheets on Ni foam (E-Co-Ni LDH/Ni foam) via a facile modified coprecipation method<sup>16</sup> followed by an effective vacuum freeze-drying technique, and (2) preparation of the end product nanoplatelet-like NiCo<sub>2</sub>O<sub>4</sub>/Ni foam by a simple thermal transformation route. Typically, specific amount of Co(NO<sub>3</sub>)<sub>2</sub> 6H<sub>2</sub>O (8 mmol) and Ni(NO<sub>3</sub>)<sub>2</sub> 6H<sub>2</sub>O (4 mmol) were dissolved in 80 mL of deionized water with 20 ml of EG. The claret solution above was then added dropwise to colorless EG containing 26 mmol NaOH under constant high-speed stirring at room temperature. After undergoing a series of Ostwald ripening, centrifuging, and washing thoroughly, the resulting reaction product was redispersed in the mixed solution including 135 mL EG and 40mL deionized water by ultrasonic vibration process to form uniform and stable suspension of E-Co-Ni LDH nanosheets. Subsequently, The bottom part (1×1 cm<sup>2</sup>) of a piece of clean nickel foam (3.5 ×1 cm<sup>2</sup>) was immersed into the dispersion for a several seconds, followed by pre-frozen treatment in liquid nitrogen and sequent vacuum freeze-drying at -60 °C under the vacuum degree of less than 10 Pa overnight. After that, the precursor E-Co-Ni LDH/Ni foam can be obtained. Next, the precursor was placed into a furnace to be annealed at a relatively low temperature of 260 °C in air for 120 min at a slow heating of 1 °C min<sup>-1</sup>, and the final nanostructure NiCo<sub>2</sub>O<sub>4</sub>/Ni foam can be achieved.

### 2.3. Characterization

The X-ray diffraction (XRD) patterns of the samples were recorded with an X-ray powder diffractometer ( $CuK_{\alpha}$ , Bruker D8). Thermogravimetric analysis and differential scanning calorimetry analysis (TG-DSC) of the powder sample were measured on the Netzsch STA 449C instrument with a heating rate of 10 °C min<sup>-1</sup> in air. The morphology of the products was characterized with a field emission scanning electron microscopy (FESEM, HITACHI S-4800) and an analytical transmission electron microscope (TEM, JEOL JEM2010) operated at 200 kV.

## 2.4. Electrochemical Measurement

Chronopotentiometry and cyclic voltammetry (CV), and electrochemical impedance spectroscopy (EIS) were conducted using a three-electrode mode in a 1 M NaOH solution on a CHI 660C electrochemistry workstation. The working electrode was nanostructure NiCo<sub>2</sub>O<sub>4</sub>/Ni foam as a binder-free electrode. The loading level of the active material was controlled to be at least 1 mg cm<sup>-2</sup>. The reference electrode and counter electrode were saturated calomel electrode (SCE) and platinum foil, respectively.

### 3. Results and Discussion

As shown in Fig. 1a, the peaks in the XRD pattern (c) of the precursor can be index to (003), (006), (101) and (110) plane reflections of both  $\alpha$ -Co(OH)<sub>2</sub> and  $\alpha$ -Ni(OH)<sub>2</sub> LDHs, <sup>16,17</sup> except for the three typical peaks originating from the Ni substrate. <sup>13</sup> A low angle reflection appears at 9.64 Å (9.17 °) followed by another reflection at about one-half this spacing, 4.78 Å (18.95 °). The interlayer distance ( $d_{003}$ 's) of ca. 9.64 Å is enlarged, compared to that (ca. 7.9 Å) reported in the literature. <sup>18</sup> Together with the coherent shift of the (00*l*) peaks, (003) and (006) plane reflections, as a whole, it can be confirmed that the precursor of EG intercalated and chemically bonded Co-Ni hydroxides was formed on the Ni foam. <sup>19-21</sup>

From the TG-DSC of the precursor powder in Fig. 1b, we can attribute the abrupt weight loss at 255–290 °C to the combustion of the intercalated EG and the decomposition of Co-Ni hydroxide into the relative oxides, while the mass loss above 290 °C to the thermal decomposition of E-Co-Ni hydroxide and the corresponding metal oxides. When the precursor E-Co-Ni LDH/Ni foam is annealed at a relatively low temperature of 260 °C, the formation of the nanostructure NiCo<sub>2</sub>O<sub>4</sub> will be accompanied by the evolution of much more gas including H<sub>2</sub>O (g) and CO<sub>2</sub> (g) from the combustion of EG. Then, it may favor the generation of porous structure, which is good for stock and penetration of the electrolyte, charge transport and ion diffusion in electrochemical reaction. As exhibited in XRD pattern (b) of the end product in Fig. 1a, the weak but distinctive, NiCo<sub>2</sub>O<sub>4</sub> reflections can be seen coming

from the (111), (311), (511), (110) reflection planes.  $^{6,16}$  The broad diffraction peaks indicate the nanosized NiCo<sub>2</sub>O<sub>4</sub> was achieved.

The FESEM images of the samples are shown in Fig. 2a-f. For the nanostructure NiCo<sub>2</sub>O<sub>4</sub>/Ni foam, the 3D grid structure with hierarchical macro-porosity of the Ni foam is well remained (Fig. 2b) and the surface is rougher than that of the pristine Ni foam (Fig. 2a). Moreover, the uniform coverage of the nanostructure NiCo<sub>2</sub>O<sub>4</sub> can be seen on the whole of the Ni foam substrate (Fig. 2d). And one can recognize that the microplate-like NiCo<sub>2</sub>O<sub>4</sub> grow on the Ni foam substrate (Fig. 2e, f).

TEM measurements were performed to investigate the inherent structural and morphological characteristics of the products (Fig. 3a-c). A nanoplatelet-like shape of the nanostructure NiCo<sub>2</sub>O<sub>4</sub> is recognized (Fig. 3a), which possesses a narrow size distribution of 2~10 nm. The nanosized NiCo<sub>2</sub>O<sub>4</sub> material provides high surface, short electron and ion transport pathways to enhance the capacitive performance.<sup>4,12</sup> A large number of mesopores and micropores can be observed in Fig. 3b and c, coming from the aggregates of the nanoplatelet-like particles (Fig. 3b) and the defects in the nanoparticles (Fig. 3c), respectively. Additionally, the diffused spotty SAED pattern with well-defined rings (in set of Fig. 3b) indicates the polycrystalline characteristics.

To further evaluate the merits of the optimal inherent microstructure and the unique architecture, we directly apply the nanoplatelet-like NiCo<sub>2</sub>O<sub>4</sub>/Ni foam as the electrode for EES. Fig. 4a shows the CV curves at various scan rates ranging from 5 to 100 mV s<sup>-1</sup> within a potential window of -0.15–0.5 V. Clearly, a pair of well-defined redox peaks is visible owing to the Faradic capacitive behavior. Their shapes have not

significantly changed with the increase of the scan rates, revealing the ideal capacitive behaviors of the nanosplatelet-like  $NiCo_2O_4/Ni$  foam.<sup>12</sup> There are battery-like voltage plateaus in the galvanic charge-discharge (CD) curves (Fig. 4b), which match well with the redox peaks in the CV curves. The corresponding specific capacitance values can be calculated by the following relationship:<sup>25</sup>

$$C_m = I \times \Delta t / \Delta V \times m \tag{1}$$

Where I is the current of charge/discharge,  $\Delta t$  is the time of discharge, and  $\Delta V$  is the potential of range, m is the mass of active electrode material (in this article  $\Delta V$ =0.45V, m=1.46 mg).

As expected, the nanosplatele-like NiCo<sub>2</sub>O<sub>4</sub>/Ni foam shows a high specific capacitance of 760 F g<sup>-1</sup> at the current density of 1 A g<sup>-1</sup> and excellent rate capacity (Fig. 4a, b, and e). The electrochemical stability of the sample was examined by repeated CV cycles at 10 mV s<sup>-1</sup>. Interestingly, the specific capacitance has been increasing before 500 cycles of fully electrochemical activation (Fig. 4c, d). The specific capacitance retention ratio reaches over 96.3 % (732.2 F g<sup>-1</sup>) after 1000 cycles based on the maximum value, indicating the unique structural stability of the sample (Fig. 4f).

As discussed before, the advantageous intrinsic structure of the nanoplatelet-like NiCo<sub>2</sub>O<sub>4</sub>/Ni foam plays a great role in the high electrochemical performance. The high specific surface affords high density of active sites to increase the redox reaction. <sup>9,26</sup> Large quantities of micro/mesopores make the mass transfer of electrolyte easier, and the interior hollow spaces may accommodate the volume change in the

redox reaction and enhance the cyclability of the electrode material as a result. 9,27,28 Simultaneously, the hybrid architecture structure is undoubtedly indispensable to the outstanding electrochemical performances, since it provides more favourable and quicker pathway for ions to penetrate owing to the direct loading of the active material on the current collector. As shown in Fig. 5, the Nyquist plot of the three-electrode system with the NiCo<sub>2</sub>O<sub>4</sub>/Ni foam electrode shows a straight line in the low-frequency region and unconspicious arc in the high frequency region, at applied potential of 0.006 V (vs SCE). The magnitude of equivalent series resistance (ESR) (0.6  $\Omega$ ) is obtained from the x-intercept of the plot for the NiCo<sub>2</sub>O<sub>4</sub>/Ni foam electrode material. The inconspicuous arc in the high frequency region indicates that the electronic resistance is low between the nanoplatelet-like NiCo<sub>2</sub>O<sub>4</sub>/Ni foam. The slope of 45° portion of the curve, called the Warburg resistance, coming from the frequency dependence of ion diffusion in the electrolyte to the electrode interface. The short Warburg curve in the plot suggests the sample has a short diffusion path, which may facilitate the efficient access of electrolyte ions to the active material surface.<sup>29</sup> Together with the facile, relative low temperature fabrication process, the high performance nanoplatelet-like NiCo<sub>2</sub>O<sub>4</sub>/Ni foam is promised to act as the candidate electrode material for widely practical applications in EES.

### 4. Conclusions

In a word, we developed a facile, green, energy-saving preparation technique to

achieve cost-effective nanostructure NiCo<sub>2</sub>O<sub>4</sub>/Ni foam for EES. The nanoplatelet-like particles of 2~10 nm provide high density active sites and advantageous porous structure for electrochemical reaction. As a binder-free electrode material, a high specific capacitance of 760 F g<sup>-1</sup> was obtained at 1 A g<sup>-1</sup> with excellent structural stability, remaining over 96.3 % after 1000 cycles. The study may facilitate the successful commercial applications of nanoplatelet-like NiCo<sub>2</sub>O<sub>4</sub>/Ni foam for high-efficient EES. The preparation architecture may be extended to other metal oxide/hydroxide-based material system for electronic, magnetic, optical, photochemical, and catalytic applications. And the relevant work is following in our further research work.

# Acknowledgements

The authors are grateful for financial support from the National Natural Science Foundation of China (Grant 51472238).

### **References**

- (1) Y. Gogotsi, P. Simon, Science, 2011, 334, 917–918.
- (2) H. Y. Chen, F. Cai, Y. R. Kang, S. Zeng, M. H. Chen, Q. W. Li, *ACS Appl. Mater. Interfaces*, 2014, **6**, 19630–19637.
- (3) J. Jiang, Y. Y. Li, J. P. Liu, X. T. Huang, C. Z. Yuan, X. W. Lou, *Adv. Mater.*, 2012, **24**, 5166–5180.
- (4) P. Simon, Y. Gogotsi, Nat. Mater., 2008, 7, 845–854.
- (5) Y. Kobayashi, X. Ke, H. Hata, P. Schiffer, T. E. Mallouk, *Chem. Mater.*, 2008, **20** 2374–2381.
- (6) S. Verma, H. M. Joshi, T. Jagadale, J. Phys. Chem. C, 2008, 112, 15106–15112.
- (7) Y. NuLi, P. Zhang, Z. P. Guo, H. K. Liu, J. Yang, *Electrochem. Solid-State Lett.*, 2008, **11**, A64–A67.
- (8) A. V. Chadwick, S. L. P. Savin, S. Fiddy, R. Alc ántara, D. F. Lisbona, P. Lavela, G.
  F. Ortiz, J. L. Tirado, *J. Phys. Chem. C*, 2007, 111, 4636–4632.
- (9) T. Y. Wei, C. H. Chen, C. C. Hu, Adv. Mater., 2010, 22, 347–351.
- (10) U. M. Patil. J. S. Sohn, S. B. Kulkarni, S. C. Lee, H. G. Park, K. V. Gurav, J. H. Kim, S. C. Jun, *ACS Appl. Mater. Interfaces*, 2014, **6**, 2450–2458.
- (11) J. Wang, Y. C. Song, Z. S. Li, Q. Liu, J. D. Zhou, X. Y. Jing, M. L. Zhang, Z. H. Jiang, *Energy Fuels*, 2010, **24**, 6463–6467.
- (12) Q. F. Wang, X. F. Wang, B. Liu, G. Yu, X. J. Hou, D. Chen, G. Z. Shen, *J. Mater. Chem. A*, 2013, **1**, 2468–2473.

- (13) C. Z. Yuan, J. Y. Li, L. R. Hou, X. G. Zhang, L. F. Shen, X. W. Lou, *Adv. Funct. Mater.*, 2012, **22**, 4592–4597.
- (14) G. Q. Zhang, H. B. Wu, H. E. Hoster, M. B. Chan-Park, X. W. Lou, *Energy Environ. Sci.*, 2012, **5**, 9453–9456.
- (15) B. Wang, G. R. Williams, Z. Chang, M. Jiang, J. F. Liu, X. D. Lei, X. M. Sun, *ACS Appl. Mater. Interfaces*, 2014, **6**, 16304–16311.
- (16) C. H. Wang, X. Zhang, D. C. Zhang, C. Yao, Y. W. Ma, *Electrochim. Acta*, 2012, **63**, 220–227.
- (17) V. Gupta, S. Gupta, N. Miura, J. Power Sources, 2008, 175, 680–685.
- (18) W. H. Chen, Y. F. Yang, H. X. Shao, J. Fan, J. Phys. Chem. C, 2008,112, 17471–17477.
- (19) Y. Li, X. W. Xie, J. L. Liu, M. Cai, J. Rogers, W. J. Shen, *Chem. Eng. J.*, 2008, **136**, 398–408.
- (20) J. J. Tunney, C. Detellier, Clays Clay Miner., 1994, 42, 552–560.
- (21) A. Kasai, S. Fujihara, *Inorg. Chem.*, 2006, **45**, 415–418.
- (22) T. Stanimirova, T. Hibino, Appl. Clay Sci., 2006, 31, 65–75.
- (23) J. C. Villegas, O. H. Giraldo, K. Laubernds, S. L. Suib, *Inorg. Chem.*, 2003, **42**, 5621–5631.
- (24) X. H. Liu, R. Z. Ma, Y. S. Bando, T. Sasaki, Adv. Mater., 2012, 24, 2148–2153.
- (25) J. J. Deng, J. C. Deng, Z. L. Liu, H. R. Deng and B. Liu, *J. Mater Sci.* 2009, **44**, 2828–2835.
- (26) Q. Wang,; D. O' Hare, *Chem. Rev.*, 2012, **112**, 4124–4155.

- (27) N. Thomas, M. Rajamathi, *Langmuir*, 2009, **25**, 2212–2216.
- (28) C. Wang, Y. Zhou, M. Y. Ge, X. B. Xu, Z. L. Zhang, J. Z. Jiang, *J. Am. Chem. Soc.*, 2010, **132**, 46–47.
- (29) Y. Wang, Z. Q. Shi, Y. Huang, Y. F. Ma, C. Y. Wang, M. M. Chen, Y. S. Chen, *J. Phys. Chem. C* 2009, **113**, 13103-13107.

# Figure captions

- Fig. 1. XRD patterns (a) of the precursor and the end product, TG-DSC curves (b) of the precursor powder.
- Fig. 2. FESEM images of Ni foam (a, c), NiCo<sub>2</sub>O<sub>4</sub>/Ni foam (b, d, e, and f).
- Fig. 3.TEM images of NiCo<sub>2</sub>O<sub>4</sub>/Ni foam (a, c), and TEM image of NiCo<sub>2</sub>O<sub>4</sub>/Ni foam (b) with corresponding SAED pattern in the inset.
- Fig. 4. CV curves at different sweep rates (a), galvanostatic charge-discharge curves at various discharge current densities (b), CV curves and charge-discharge curves after undergoing a serious of CV cycles at 10 mV s<sup>-1</sup>, respectively (c, d), average specific capacitance at various discharge current densities (e) and stability test in terms of specific capacitance at 1 A g<sup>-1</sup> by CV cycles at 10 mV s<sup>-1</sup> (f) of NiCo<sub>2</sub>O<sub>4</sub>/Ni foam.
- Fig. 5. Nyquist plots for  $NiCo_2O_4/Ni$  foam electrode material at applied potential of 0.006 V (vs SCE). Z': real impedance. Z": imaginary impedance. Inset shows an enlarged scale.

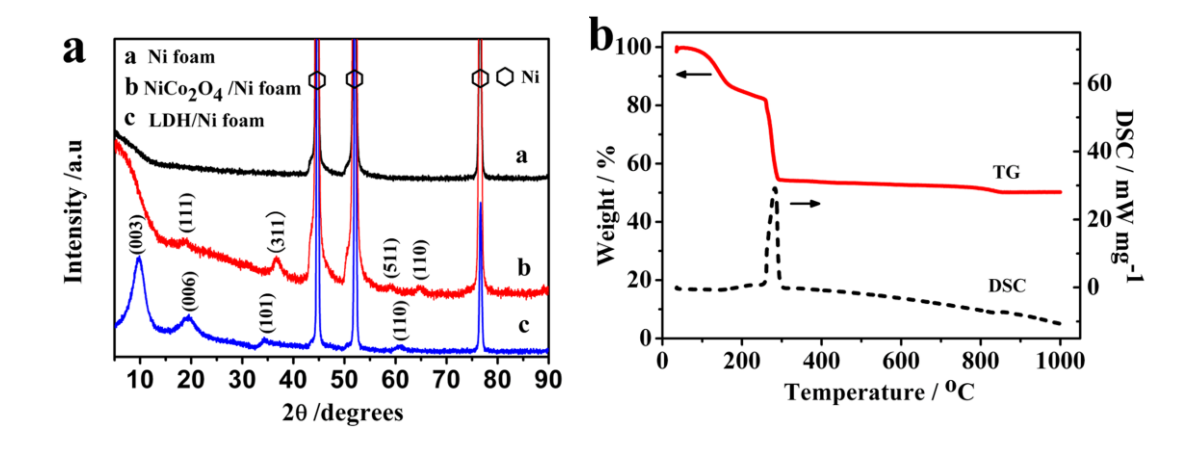


Fig. 1.

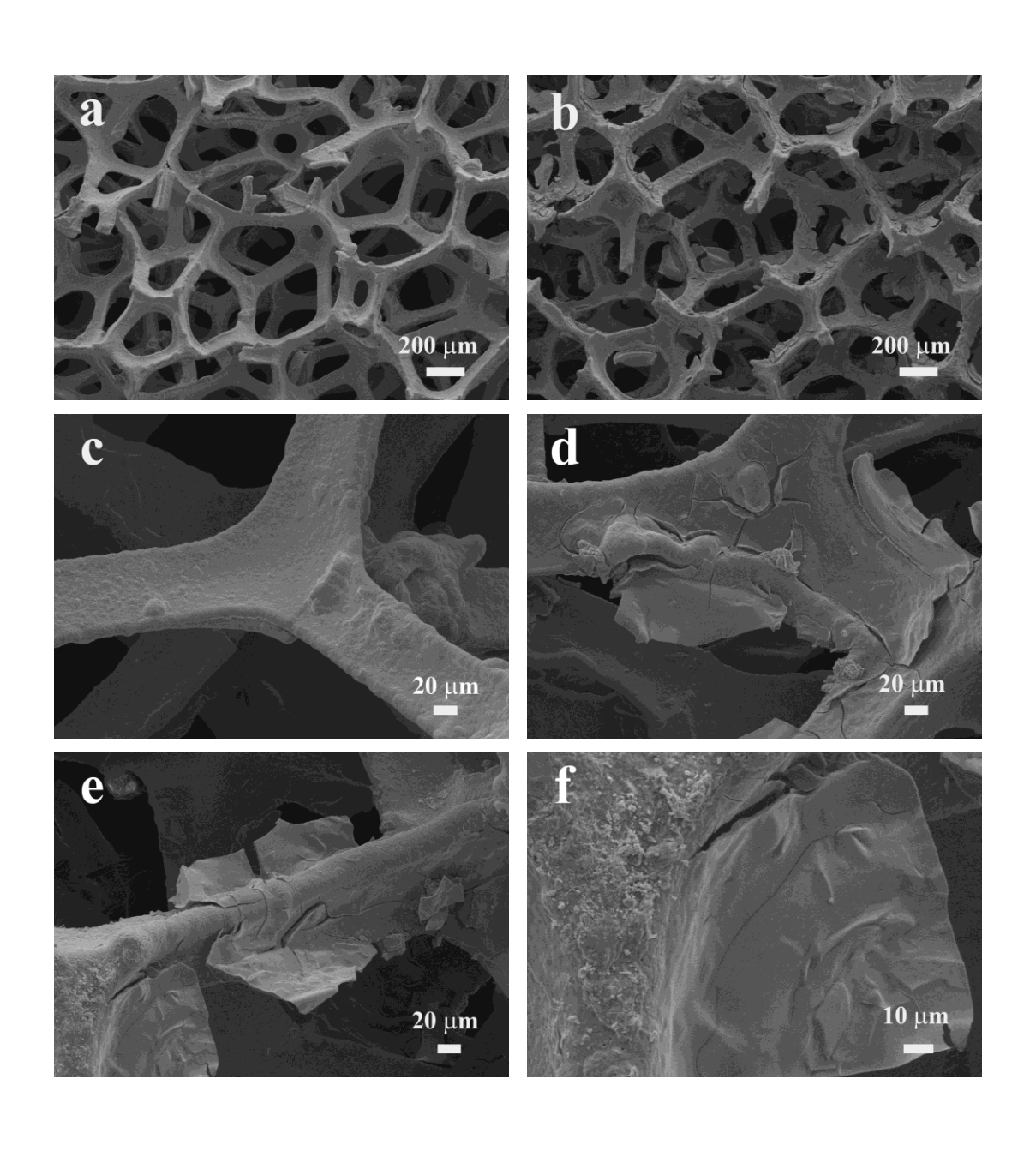


Fig. 2

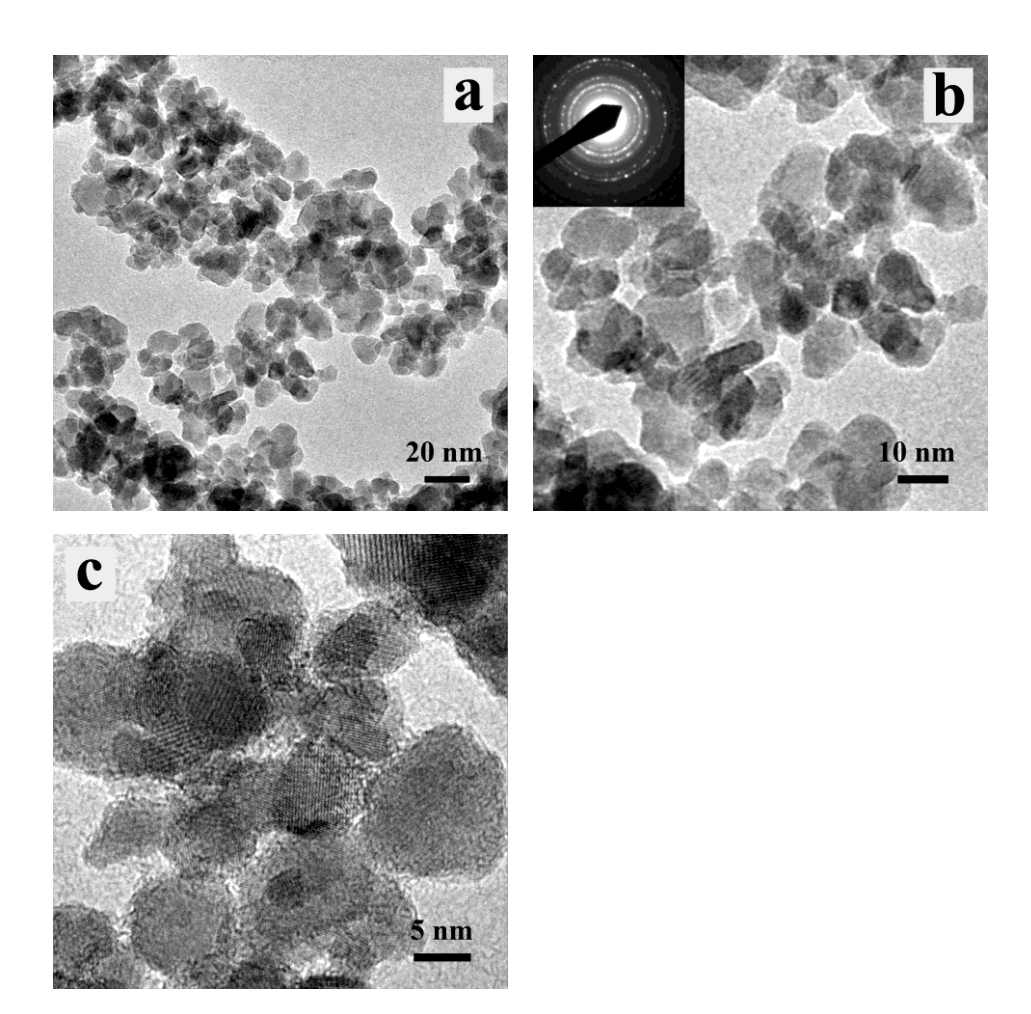


Fig. 3.

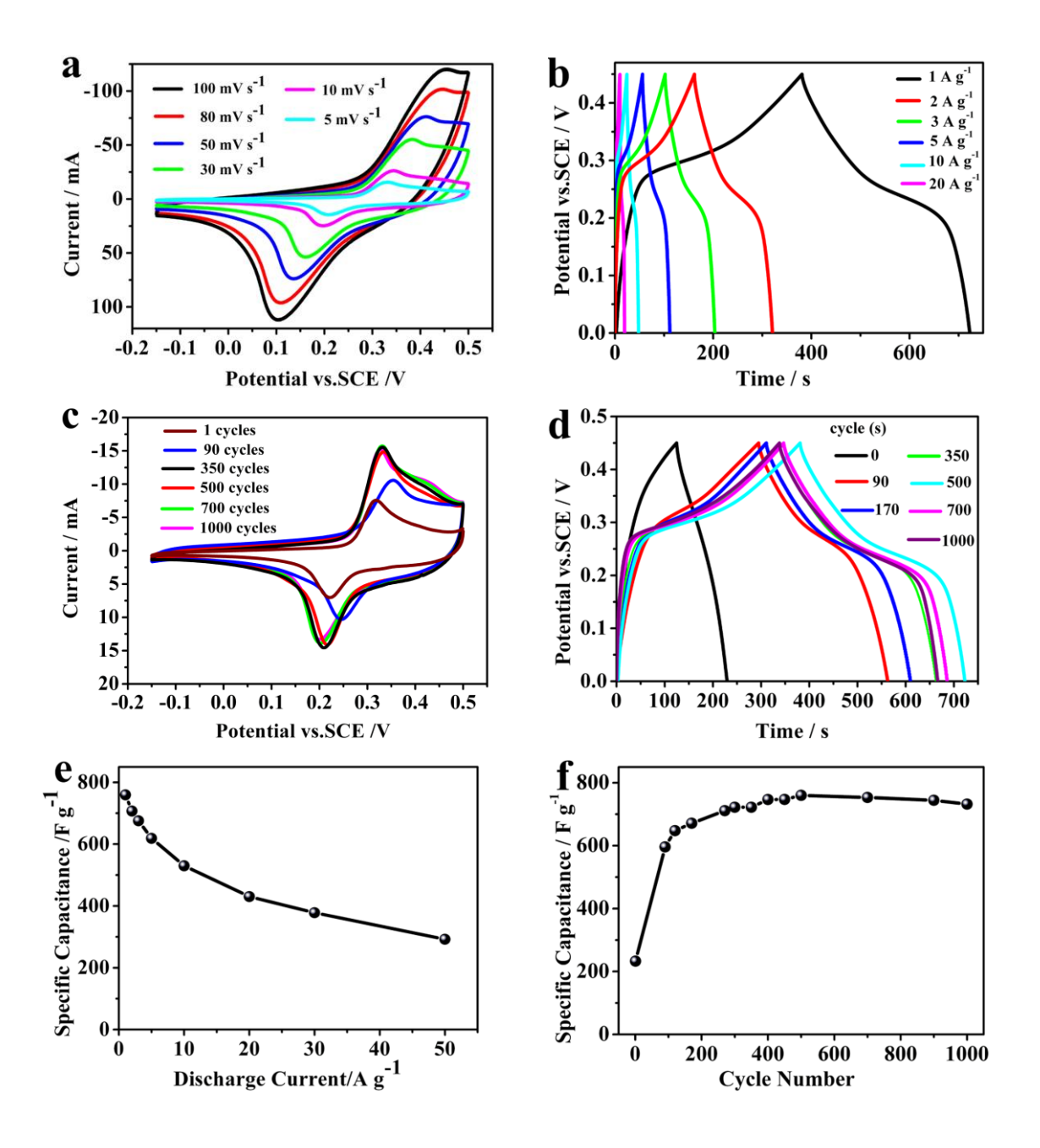


Fig. 4.

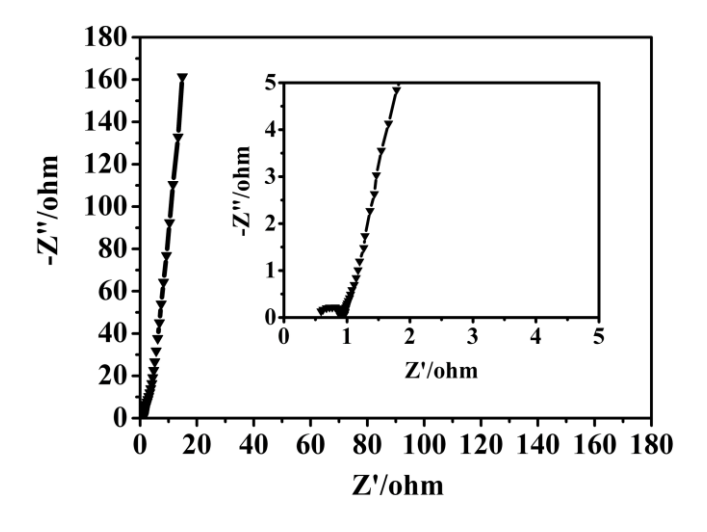


Fig. 5